Revisiting the fingerprint of organic matters in speleothem by Electron Paramagnetic Resonance

Yves Perrette, Hervé Vezin, Bernard Fanget, Julia Garagnon, Jérome Poulenard

Organic Geochemistry 201 (2025) 104929

Contents lists available at ScienceDirect

Organic Geochemistry

journal homepage: www.elsevier.com/locate/orggeochem

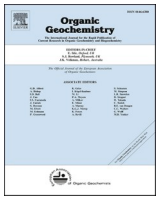

Revisiting the fingerprint of organic matters in speleothem by Electron Paramagnetic Resonance☆

Yves Perrette [a,*], Hervé Vezin [b], Bernard Fanget [a], Julia Garagnon [a], Jérome Poulenard [a]

[a] Univ. Savoie Mont-Blanc, CNRS, EDYTEM, Bâtiment Pole Montagne, Campus Scientifique, F-73376 Le Bourget du Lac Cedex, France
[b] Univ. Lille, CNRS, UMR 8516, LASIRe, F-59000 Lille, France

ARTICLE INFO

Associate Editor — Paul Francis Greenwood

Keywords:
Soil organic matter
Electron Paramagnetic Resonance spectroscopy
UV fluorescence spectroscopy
Speleothems

ABSTRACT

The evolution of soil organic carbon (SOC) stocks is critical for both food production and climate change mitigation. This study uses advanced electron paramagnetic resonance (EPR) spectroscopy to investigate the spatial localisation and characterisation of organic carbon in speleothems, with a particular focus on methodological advances in recent decades. A speleothem sample from the Choranche cave in France was analysed using UV laser-induced fluorescence (LIF) and continuous wave EPR spectroscopy. The LIF analysis identified three main types of organic compounds – aromatic amino acids, aliphatic aromatics and larger aromatic compounds – distributed throughout the sample. EPR spectroscopy revealed the presence of Fe^{3+} and Mn^{2+} ions, along the entire sample for Fe^{3+} and more localised for Mn^{2+}. When radical organic matter (ROM) is detected, first and second harmonic EPR imaging shows its collocation with Fe^{3+} and Mn^{2+}, suggesting specific embedding conditions or source events. The study highlights a significant discrepancy between fluorescent organic matter (FOM) and ROM, challenging previous assumptions about their co-transfer from soil to speleothems. The results suggest that ROM is likely to be associated with specific soil redox conditions or high-energy events, whereas FOM represents a continuous background transfer. This distinction is crucial for accurate interpretations of soil organic carbon loss and its environmental implications. Future research should integrate detailed spectroscopic and isotopic analyses to better quantify organic carbon dynamics and their environmental proxies. Our results highlight the importance of distinguishing between different types of organic matter in speleothems to improve our understanding of soil organic carbon fluxes in relation to climate and human land use.

1. Introduction

The evolution of soil organic carbon stocks is essential for both food production and climate change mitigation, particularly concerning greenhouse gas concentrations in the atmosphere. Soil organic matter, along with the organic carbon fluxes derived from it, plays a crucial role in the ecological functioning of numerous terrestrial and aquatic environments (Schmidt et al., 2011). In anthropogenic systems, especially agriculture, changes in soil organic matter—both in quantity and quality—serve as excellent indicators of soil evolutionary trajectories and reflect the relationship between the environment and human society.

Soil organic matter should therefore be consistently monitored. Relying solely on short-term observations can lead to misinterpretations of current conditions. Organic matter flux should be examined over secular or millennial time scales to better understand its relationship with climate and anthropogenic land-use changes (Pearson et al., 2024). Natural archives, such as carbonates or sediments, can provide a record of organic flux over time. Organic matter has been studied as a proxy for climate, soil, and environmental changes since the early works of White (1981). The still-relevant review by Blyth et al. (2016) outlines knowledge regarding the sources and various organic proxies used in speleothems.

Continuous Wave Electron Paramagnetic Resonance (CW-EPR) spectroscopy has shown significant promise in tracing and characterizing the sources of organic matter from soils and its transfer through karst systems (Perrette et al., 2000, 2015). To explore the relationship between anthropogenic land use and organic matter fluxes from soils, this initial source-to-sink approach must be supplemented with more qualitative analysis. This would enhance our understanding of the types of organic compounds present, such as distinguishing between different

☆ This article is part of a special issue entitled: 'Organic geochemistry and archaeology' published in Organic Geochemistry.

* Corresponding author.
E-mail address: yves.perrette@cnrs.fr (Y. Perrette).

https://doi.org/10.1016/j.orggeochem.2025.104929
Received 23 July 2024; Received in revised form 2 January 2025; Accepted 2 January 2025
Available online 6 January 2025

types of amino compounds, and comprehending the spatial and potentially functional relationships between organic and inorganic compounds associated with karst waters (Hartland et al., 2012).

Since our initial work (Perrette et al. 2015), significant methodological and technological advancements have been made in EPR spectroscopy, enabling us to deepen our understanding of organic matter (OM) trapped in calcites. In our previous research, EPR spectroscopy was conducted on calcite powders. Additionally, the use of powders limited spatial interpretation (i.e., temporal interpretation for natural archives), as 10 g of calcite were required. Our earlier work focused exclusively on semiquinonic free radicals at that time to trace OM from soils to speleothems.

Our aim now is to present the new insights that modern EPR spectroscopy can offer, utilizing spectral-spatial and 2D EPR imaging (spectral-spatial and spatial/spatial) to describe the spatial distribution of different types of organic carbon.

To highlight the value of these new capabilities, we focus on the subaqueous flowstone sample analyzed in our previous work (Perrette et al., 2015). In this study, we emphasize the methodological advancements in EPR spectroscopy, without delving into the chronology of the OM record.

2. Materials

The speleothem studied was sampled from the Choranche show cave (France, 45.07° N, 5.4° E, 610 m above sea level). A detailed description of the calcite sample is available in Perrette et al. (2015). Briefly, it is a subaqueous flowstone (Hill and Forti, 1997) constantly moistened by flowing water from the "Chevaline" subterranean river in the "Serpentine" passage. It is characterized by a growth rate of 500 μm/year, which was estimated from observations of calcite growth on glass plates in the cave (Delannoy, 1982). The calcite studied here was formed over the last few decades (SI 1).

3. Methods

3.1. UV laser-induced fluorescence

UV laser-induced fluorescence (LIF) was measured using a Nd-YAG laser emitting the quadrupled frequency at 266 nm (CryLas). The diffuse spectrofluorescence was analyzed using a monochromator (MicroHR, Jobin Yvon) equipped with an adjustable slit and a 300 g/mm diffraction grating centered at 600 nm, providing approximately 1 nm/px spectral resolution. The signal was detected with a back-illuminated CCD (Sincerity, Jobin Yvon). This setup enabled the acquisition of hyperspectral images via a two-axis translation stage. A 50 × 50 μm step size was used to analyze the sample.

3.2. EPR experiments

Continuous Wave Electron Paramagnetic Resonance (CW-EPR) experiments were conducted using an E580 EPR spectrometer operating at X-band. Spectra were recorded at room temperature with a TMS low-Q resonator, enabling measurements across the entire sample. The CW EPR spectra were obtained with microwave power set to 2 mW and modulation amplitude to 1 G. Data were collected to achieve a signal-to-noise ratio greater than 20 dB.

EPR imaging was performed using a 2D YZ-axis gradient with a gradient strength of 175 G/cm and a field of view of 20 mm. The image was collected with 512 pixels on each axis, resulting in 402 angles. The final pixel size of approximately 40 μm corresponds to roughly 9 months of speleothem growth, considering the growth rate of 500 μm/year. 1D spectral-spatial imaging along the Y-axis was performed under the same conditions. Image reconstruction was carried out using the back-projection method, with prior spectral deconvolution for the 2D spatial image.

Additionally, the 2D spectral-spatial images were acquired in both first and second harmonics. Given the significant contribution of metals (Mn and Fe), the second harmonic technique was used to enhance signals with the longest transverse relaxation times (T2e), since line width is inversely proportional to T2e. This approach allowed the detection of organic matter (OM) contributions not visible in the first harmonic. The residual Mn^{2+} signal was used to align the images acquired in both detection modes.

4. Results

4.1. UV spectrofluorescence

The spectrofluorescence of the sample shows a broad emission spectrum across the entire sample. This fluorescence has been widely attributed to organic materials (White, 1981) and can be modeled by the linear combination of log-normal functions, which correspond to aromatic amino acids (350 nm; shaded green in Fig. 1), aromatics with some aliphatic chains (450 nm; light blue), and larger aromatic compounds (550–600 nm; dark blue). These compounds are commonly referred to as protein-like, fulvic-like, and humic-like, respectively (Moya et al., 2023). The average spectrum (Fig. 1) displays the different log-normal functions after spectral simulation of the fluorescence map for the entire sample (SI-2). Three types of organic compounds—aromatic amino acids (λem. 350 nm), aromatics with aliphatic chains (λem. 450 nm), and larger aromatic compounds (λem. 550–600 nm; purple in Fig. 1)—are observed throughout the sample, with both qualitative and quantitative variations along the speleothem bands (Baker et al., 1993; Quiers et al., 2015).

4.2. EPR Spectroscopy

In organic geochemistry, EPR spectroscopy has traditionally been limited to detecting organic matter after grinding the sample. However, this new technique allows for the analysis of native samples without alteration, and the EPR detection of all paramagnetic elements, such as manganese and iron.

The EPR spectrum of the sample recorded at room temperature reveals a complex set of signals over a field range of 6000 G (Fig. 2a), predominantly showing high concentrations of Fe^{3+} ions, present as isolated complexes ($g = 4.3$) and iron oxide aggregates with very broad lines (width > 500 G). A set of six lower-intensity lines is also visible. Fig. 3 shows this spectrum acquired with a sweep width of 700 G and highlight six distinct lines separated by 85 G. These lines are characteristic of manganese ions (Mn^{2+}, $S = 5/2$, $I = 5/2$) when it is substituted for calcium in calcite. The 85 G separation reflects the hyperfine coupling between the electronic and nuclear spins of manganese. This manganese spectrum also exhibits the two forbidden transitions between the allowed ones. In the center of the spectrum, a faint signal between the two forbidden transitions suggests the presence of organic radicals (red R° in Fig. 3).

To confirm this, a spectrum was recorded with a smaller sweep width of 50 G. Fig. 4 shows the presence of two types of organic signals: monoradicals ($S = 1/2$) and biradicals ($S = 1$). The monoradicals exhibit g-factors of $g = 2.0036$ and $g = 2.0073$, which can be attributed to carbon radicals. The biradical signal ($S = 1$) arises from the dipolar interaction between two electron pairs.

The zero-field coupling (ZFS) value between the two electrons is measured at 20 G. This 20 G (56 MHz) dipolar interaction indicates a structure where the two electrons are separated by approximately 0.95 nm. If we assume the EPR signal represents the entire distribution of species in the sample, the total concentration of radicals and biradicals is estimated to be around 4×10^{14} spins/g.

To spatially locate these species within the sample, we performed two types of EPR imaging experiments (Fig. 5). First, we acquired a one-dimensional image along the spatial axis as a function of the spectral

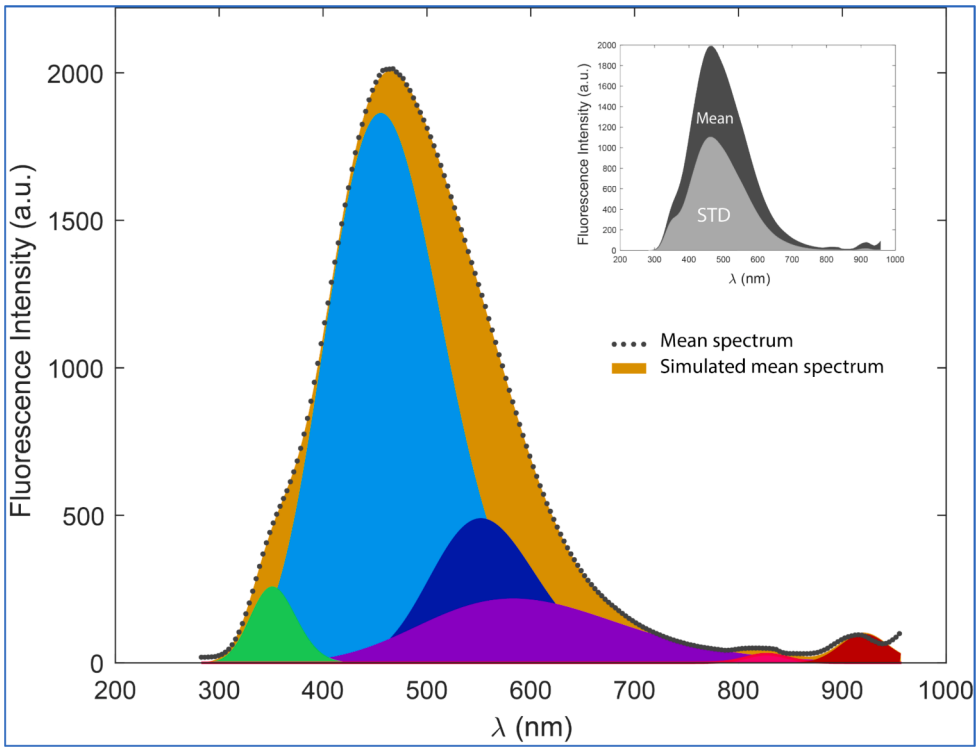

Fig. 1. Spectrofluorescence emission spectrum of the subaqueous flowstone with fluorophore simulations and the standard deviation of fluorescence for the entire sample (SI-2). The last two contributions (in red; Nb. not referred to in the text) are infrared reflectances induced by laser emission (YAG). (For interpretation of the references to color in this figure legend, the reader is referred to the web version of this article.)

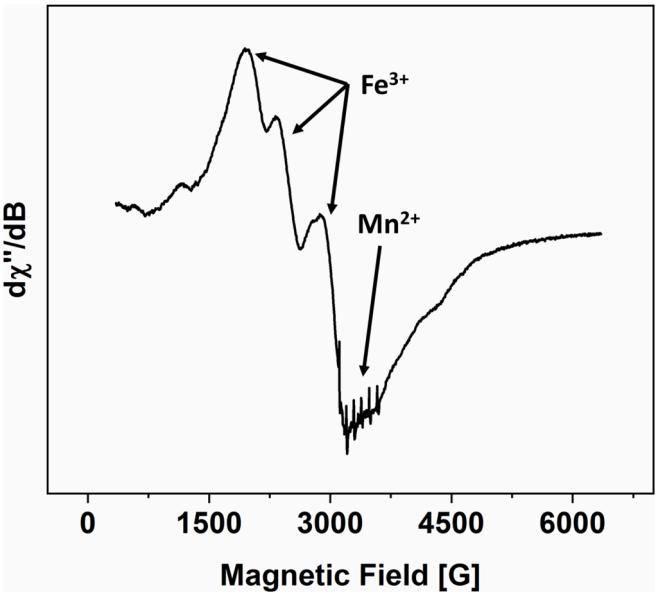

Fig. 2. EPR spectra of Fe^{3+} and Mn^{2+} from the entire CHO core (20 × 6 mm) recorded at room temperature. Spectra were acquired with a sweep width of 6000 G.

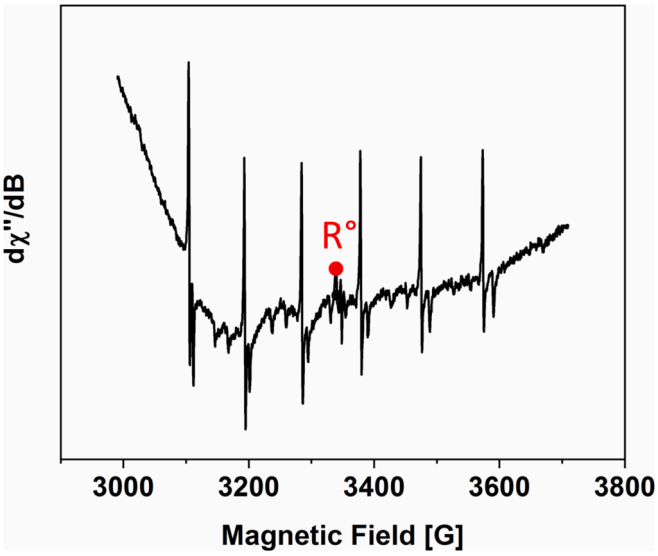

Fig. 3. EPR spectra of organic radicals from the entire CHO core (20 × 6 mm) recorded at room temperature. Spectra were acquired with a sweep width of 700 G.

dimension, tracing the concentration profile of each species along the core. Image 5a corresponds to a spectral width of 2400 G designed to detecte Fe^{3+} (in green on Fig. 5a). The iron oxide species appear homogeneously distributed throughout the sample. In contrast, Mn^{2+} species are highly localized in two specific regions of the sample. The region identified by a black rectangle in Fig. 5a indicates the detection of the Mn^{2+} lines, and an expanded view of these signals are shown in Fig. 5 b. Unlike Fe^{3+}, Mn^{2+} is mainly located in two distinct layers from 12 to 14 mm from the top of the sample. However, with this acquisition method, it was not possible to localize organic matter, as it does not significantly contributes to the total EPR signal.

To localize the organic matter, we acquired two 2D spectral/spatial images using two EPR detection modes. The image acquired in the first harmonic mode (Fig. 5 C) reveals the spatial distribution of manganese mainly in two 600 μm zones along the axis of the sample, spanning the entire 6 mm cross-section. Outside these two zones, a small distribution

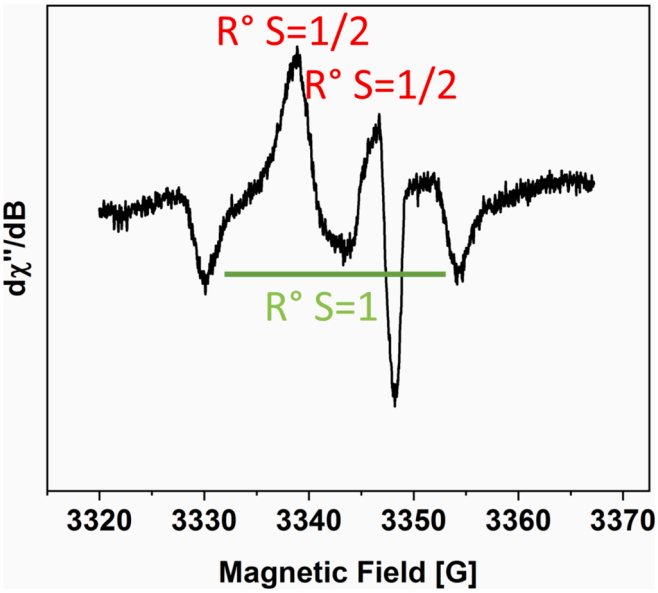

Fig. 4. EPR spectra of the entire CHO core (20 × 6 mm) recorded at room temperature. Spectra were acquired with a sweep width of 50 G.

representing low concentration of Mn^{2+} is also visible. To enhance the ratio of organic to manganese signals, we used a second-harmonic detection mode, which selects for longer transverse relaxation times (T2). By optimizing the microwave power and combining it with this detection mode, we were able to saturate the manganese signals and enhance the organic radical signals. Organic radicals are still detected in the Mn^{2+} layers observed in Fig. 5 C, but three more distinct islands of organic matter, associate with low concentrated manganese regions, were observed. These islands, varying in size (1 × 1 mm, 0.8 × 0.09 mm, and 0.9 × 0.3 mm), are highly localized and heterogeneously distributed. Some low manganese areas of the first harmonic 2D spatial (Fig. 5 C dotted elipses) are not co-located with organic radicals of Fig. 5 D.

This new imaging technique allows us to spatially locate organic matter in the sample and explore its co-localization with other elements.

5. Discussion

5.1. Discrepancy between organic fluorescent background and organic radicals

Unlike our previous study (Perrette et al., 2015), where EPR measurements were performed on powdered samples, this study involved direct EPR analysis on the intact sample. The present results clearly highlight the distinction between fluorescent organic matter (FOM) and free-radical organic matter (ROM). While FOM is evenly distributed across the sample, forming a background layer, ROM is highly localized

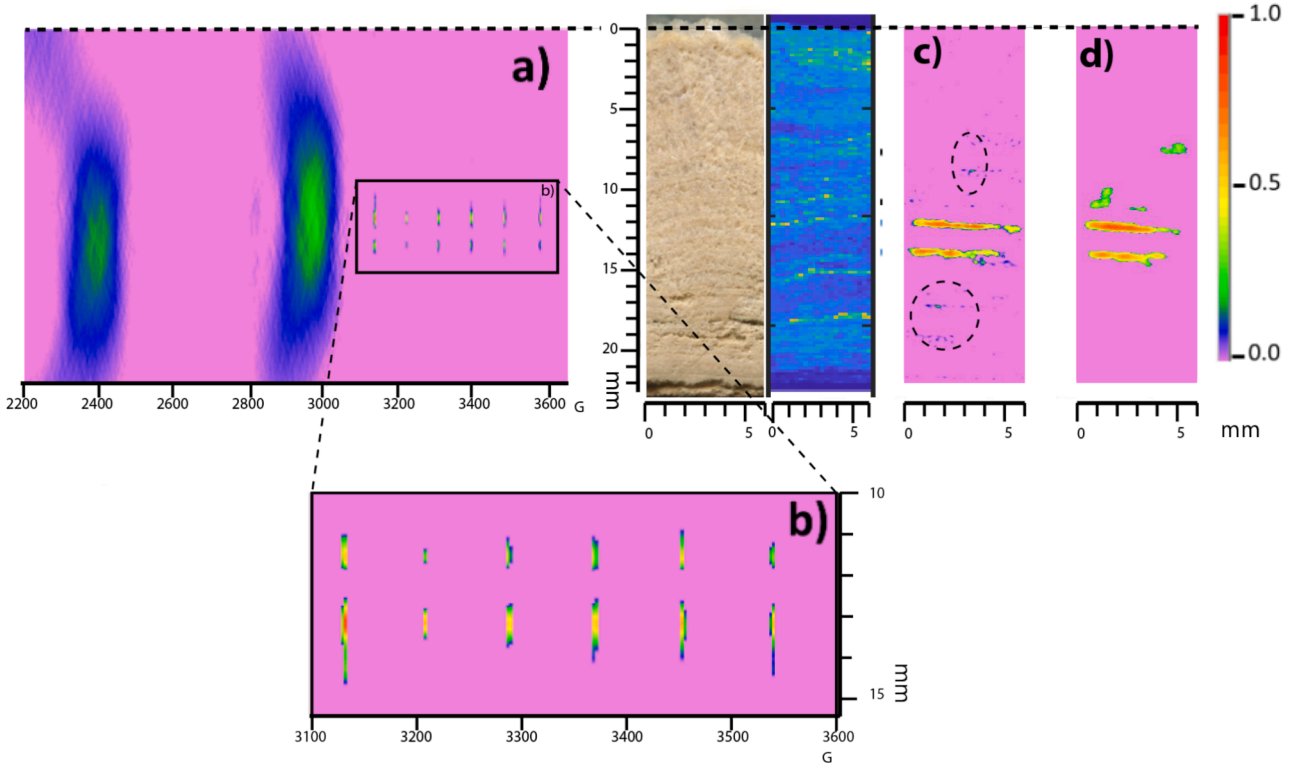

Fig. 5. EPR imaging experiments:
– Center image: fluorescence map of the sample (blue to yellow indicating low to high intensities).
– (a) 1D spectral/spatial image (512 pixels, resolution of 40 μm per pixel) with a spectral width of 2400 G along the spectral dimension, showing the Fe^{3+} signal and Mn^{2+} from 12 to 14 mm from the top.
– (b) 1D spectral/spatial zoomed to a spectral width of 500 G along the spectral dimension, highlighting the Mn^{2+} signal area.
– (c) 2D YZ spectral/spatial image in the first harmonic (image size of 512 × 512 pixels, resolution of 40 μm per pixel), showing the spatial distribution of Mn^{2+}. Dotted ellipses show the low Mn^{2+} signals which do not co-located with ROM image.
– (d) 2D YZ spectral/spatial image in the second harmonic (image size of 512 × 512 pixels, resolution of 40 μm per pixel), showing the distribution of organic radicals which do co-locate with Mn^{2+}.
For (a-d) images the same colorscale is used. Pink color indicates no signal (zero, close to experimental noise) and colored are scaled from blue (low signal) to red (high signal).

and co-occurs with trace metal enrichments (Mn). The source and transport mechanisms of FOM have been extensively studied and discussed since White's pioneering work (White, 1981). Our current results align with the well-established understanding of FOM being transported from soil sources through seepage waters and eventually incorporated into calcite (Blyth et al., 2016b). However, ROM behaves differently. The co-location of ROM consistently with Fe^{3+} and more sporadically with Mn^{2+} suggests it may represent either (i) a specific source or event or (ii) particular conditions during its incorporation into calcite.

(i) Source explanation: Metal ions are widely present in the environment (Carretero and Kruse, 2015; Suada Luzati et al., 2016). In earlier work, Mn^{2+} signatures in calcite were interpreted as proxies for oxido-reductive conditions in soils (Perrette et al., 2000). The reduction of Mn^{4+} to Mn^{2+} enables its transport in water, implying that organic matter and Mn^{2+} could be transferred during episodes of high soil moisture. In this study, we also observed ferric ions (Fe^{3+}) in the calcite, despite expectations of detecting ferrous ions (Fe^{2+}). Studies have shown that soluble organic complexes with Fe^{3+} can form under suboxic conditions in sedimentary environments (Jones et al., 2011). Such Fe-OM complexes could account for the simultaneous transport of oxidized Fe^{3+} with organic matter and reduced Mn^{2+}.

(ii) Sink production of ROM-Fe^{3+}-Mn^{2+}: Microbial mineralization of organic matter is known to be efficient when coupled with the reduction of Mn^{4+} and Fe^{3+} oxides under anaerobic conditions (Lovley, 1991). As indicated by the background UV fluorescence, organic matter is consistently present in the sample. A biofilm may form when water flow decreases, allowing microbial activity to thrive, particularly during warmer periods. This could result in the microbial generation of free radicals in organic matter, the reduction of Mn^{4+} oxides, and the incorporation of Mn^{2+} into the calcite lattice. This scenario may also involve the reduction of Fe^{3+} to Fe^{2+}, although this was not observed. It is also unlikely that the presence of specific microbial communities would selectively influence these processes in natural environments. Iron ions are known to affect calcite growth, either inhibiting it in the case of Fe^{2+} or acting as nuclei for FeO(OH) (Mejri et al., 2015). However, petrographic observations do not suggest any significant changes in calcite growth induced by the presence of Fe^{2+}. Moreover, Fig. 5 (C and D) shows two localized inclusions of ROM and metal ions, possibly linked to local reductions of Mn, the formation of free radicals, and the incorporation of OM-Fe^{3+} complexes.

ROM also reveals the presence of stable bi-radicals, which are typically produced in high-energy environments, such as during fires. Charcoal burning over the past centuries and atmospheric soot are likely sources of bi-radical ROM (Elias et al., 2023, 2024). Therefore, the interpretation of a soil source remains the most explanation, pointing to reducing conditions with the transfer of Mn^{2+} and organic-Fe^{3+} complexes from soils, along with radical organic matter. However, we cannot yet determine whether Fe^{3+} is complexed with ROM or FOM before its incorporation into calcite.

5.2. Insights into OM interpretation as environmental proxies in subaqueous flowstones

Our previous interpretations of ROM as a soil fingerprint were based on the assumption of co-location and co-transfer of ROM and FOM. This study, however, demonstrates that ROM and FOM represent distinct types of organic matter. ROM, with its bi-radicals and association with oxidized Fe^{3+} and reduced Mn^{2+}, is more clearly linked to soil processes, while FOM is more widely distributed and not as readily associated with a specific soil source. The separation of ROM and FOM in flowstones calls for a reassessment of our previous conclusions, particularly regarding the cambisol and organosol soils contributing to the ROM signature in flowstones.

The results suggest that ROM may be transferred during high-discharge events, such as snowmelt, aligning with earlier interpretations of flood events leading to increased concentrations of free radicals. In contrast, FOM, which is consistently present, cannot yet be linked to a specific soil type.

The use of OM content in speleothems as a proxy for soil organic carbon (SOC) loss due to anthropogenic activities and climate change has been well-documented (Adhikari and Hartemink, 2016; Blyth et al., 2016b; Pearson et al., 2024). However, this study reveals that traditional methods of organic carbon quantification, which often involve acid digestion of calcite, may conflate ROM and FOM contributions. As such, previous estimates of SOC fluxes in speleothem studies should be revisited with caution, particularly given the distinct transfer mechanisms of ROM (event-driven) versus FOM (continuous).

Although the aromatic characteristics of FOM and ROM trapped in calcite suggest mobility, the stability of SOC depends on factors such as water saturation and accessibility within soil aggregates (Schmidt et al., 2011). Continuous fluorescence measurements in this study indicate ongoing loss of water-extractable organic carbon, supporting previous findings that lateral water flows reduce humic organic carbon in steeper soils (González-Domínguez et al., 2019).

The ROM signal, representing organo-metallic complexes, implies that these chelated forms of organic matter are also transferred during specific high-discharge events. However, it remains challenging to quantify the relative contributions of ROM and FOM to overall organic carbon loss based on speleothem records (Quiers et al., 2015). While FOM appears throughout the sample, ROM's bi-radical content suggests the presence of highly condensed carbon material that could influence the organic carbon budget. To address this, future studies should include micromilling of calcite layers with varying ROM content, alongside isotopic and organic carbon quantifications (Blyth et al., 2013).

Further analytical developments, such as μ-Raman spectroscopy (Henry et al., 2018) and advanced EPR measurements, could help to explore the atomic structure and neighborhood of OC (Elias et al., 2023).

6. Conclusions:

This study presents the first application and interest of 2D EPR imaging to the analysis of calcite in speleothem samples. The results highlight the spatial distribution of free-radical organic matter in areas of high concentration, separated from zones enriched in fluorescent organic matter. These contrasting spatial distributions should alert us to the existence of source zones and distinct transfer processes between these two types of organic matter trapped in speleothems. These results emphasize the importance of high-resolution spatial approaches to the study of organic matter in stalagmites and the need for great care in their environmental interpretation.

CRediT authorship contribution statement

Yves Perrette: Writing – original draft, Validation, Investigation, Funding acquisition, Formal analysis, Data curation, Conceptualization. **Hervé Vezin:** Writing – review & editing, Writing – original draft, Methodology, Formal analysis, Data curation, Conceptualization. **Bernard Fanget:** Writing – review & editing, Investigation. **Julia Garagnon:** Writing – review & editing, Investigation, Formal analysis. **Jérome Poulenard:** Writing – review & editing, Investigation.

Declaration of competing interest

The authors declare the following financial interests/personal relationships which may be considered as potential competing interests: PERRETTE Yves reports financial support was provided by French National Research Agency. If there are other authors, they declare that they have no known competing financial interests or personal relationships that could have appeared to influence the work reported in this paper.

Acknowledgments

The fluorescence setup used in this work was developed by the ANR LabCom 18-LCV2-0006-01. EPR measurements were achieved by the support of the research infrastructure of the CNRS Infranalytics FR2054. We acknowledge the Grottes de Choranche for the authorization to sample the subaqueous flowstone used in that study and Stéphane JAILLET for the use photo added in supplementary informations. We would like to thank Andy Baker, the second anonymous reviewer and the editors Paul Greenwood and Elizabeth Minor for their reviews and suggestions, which have greatly contributed to improving the quality of this manuscript

Appendix A. Supplementary data

Supplementary data to this article can be found online at https://doi.org/10.1016/j.orggeochem.2025.104929.

Data availability

Data will be made available on request.

References

Adhikari, K., Hartemink, A.E., 2016. Linking soils to ecosystem services — a global review. Geoderma 262, 101–111.
Baker, A., Smart, P.L., Edwards, R.L., Richards, D.A., 1993. Annual growth banding in a cave stalagmite. Nature 364, 518–520.
Blyth, A.J., Hartland, A., Baker, A., 2016b. Organic proxies in speleothems – New developments, advantages and limitations. Quaternary Science Reviews 149, 1–17.
Blyth, A.J., Shutova, Y., Smith, C., 2013. δ13C analysis of bulk organic matter in speleothems using liquid chromatography–isotope ratio mass spectrometry. Organic Geochemistry 55, 22–25.
Blyth, A.J., Hartland, A., Baker, A., 2016a. Organic proxies in speleothems – new developments, advantages and limitations. Quaternary Science Reviews 149, 1–17.
Carretero, S., Kruse, E., 2015. Iron and manganese content in groundwater on the northeastern coast of the Buenos Aires Province, Argentina. Environmental Earth Sciences 73, 1983–1995.
Delannoy, J.-J., 1982. La karstographie souterraine. Revue Belges De Géographie 1, 61–68.
Elias, J., Faccinetto, A., Vezin, H., Mercier, X., 2023. Investigation of resonance-stabilized radicals associated with soot particle inception using advanced electron paramagnetic resonance techniques. Communications Chemistry 6, 99.
Elias, J., Faccinetto, A., Irimiea, C., Nuns, N., Pirim, C., Focsa, C., Vezin, H., Mercier, X., 2024. On the chemical composition and structure of incipient soot in a laminar diffusion flame. Fuel 373, 132056.
González-Domínguez, B., Niklaus, P.A., Studer, M.S., Hagedorn, F., Wacker, L., Haghipour, N., Zimmermann, S., Walthert, L., McIntyre, C., Abiven, S., 2019. Temperature and moisture are minor drivers of regional-scale soil organic carbon dynamics. Scientific Reports 9, 6422.
Hartland, A., Fairchild, I.J., Lead, J.R., Borsato, A., Baker, A., Frisia, S., Baalousha, M., 2012. From soil to cave: Transport of trace metals by natural organic matter in karst dripwaters. Chemical Geology 304, 68–82.
Henry, D.G., Jarvis, I., Gillmore, G., Stephenson, M., Emmings, J.F., 2018. Assessing low-maturity organic matter in shales using Raman spectroscopy: Effects of sample preparation and operating procedure. International Journal of Coal Geology 191, 135–151.
Hill, C., Forti, P., 1997. Cave minerals of the world. NSS ed.
Jones, M.E., Beckler, J.S., Taillefert, M., 2011. The flux of soluble organic-iron(III) complexes from sediments represents a source of stable iron(III) to estuarine waters and to the continental shelf. Limnology and Oceanography 56, 1811–1823.
Lovley, D.R., 1991. Dissimilatory Fe(III) and Mn(IV) reduction. Microbiological Reviews 55, 259–287.
Mejri, W., Ben Salah, I., Tlili, M.M., 2015. Speciation of Fe(II) and Fe(III) effect on $CaCO_3$ crystallization. Crystal Research and Technology 50, 236–243.
Moya, A., Giraud, F., Molinier, V., Perrette, Y., Charlet, L., Van Driessche, A., Fernandez-Martinez, A., 2023. Exploring carbonate rock wettability across scales: Role of (bio) minerals. Journal of Colloid and Interface Science 642, 747–756.
Pearson, A.R., Fox, B.R.S., Hellstrom, J.C., Vandergoes, M.J., Breitenbach, S.F.M., Drysdale, R.N., Höpker, S.N., Wood, C.T., Schiller, M., Hartland, A., 2024. Warming drives dissolved organic carbon export from pristine alpine soils. Nature Communications 15, 3522.
Perrette, Y., Delannoy, J.-J., Bolvin, H., Cordonnier, M., Destombes, J.-L., Zhilinskaya, E. A., Aboukais, A., 2000. Comparative study of a stalagmite sample by stratigraphy, laser induced fluorescence spectroscopy, EPR spectrometry and reflectance imaging. Chemical Geology 162, 221–243.
Perrette, Y., Poulenard, J., Protière, M., Fanget, B., Lombard, C., Miège, C., Quiers, M., Nafferchoux, E., Pépin-Donat, B., 2015. Determining soil sources by organic matter EPR fingerprints in two modern speleothems. Organic Geochemistry 88, 59–68.
Quiers, M., Perrette, Y., Chalmin, E., Fanget, B., Poulenard, J., 2015. Geochemical mapping of organic carbon in stalagmites using liquid-phase and solid-phase fluorescence. Chemical Geology 411, 240–247.
Schmidt, M.W.I., Torn, M.S., Abiven, S., Dittmar, T., Guggenberger, G., Janssens, I.A., Kleber, M., Kögel-Knabner, I., Lehmann, J., Manning, D.A.C., Nannipieri, P., Rasse, D.P., Weiner, S., Trumbore, S.E., 2011. Persistence of soil organic matter as an ecosystem property. Nature 478, 49–56.
Suada, Luzati, Arjan, Beqiraj, Enkeleida, Beqiraj Goga, Olgert, Jaupaj, 2016. Iron and Manganese in Groundwater of Rrogozhina Aquifer, Western Albania. Journal of Environmental Science and Engineering B 5, 276–285. https://doi.org/10.17265/2162-5263/2016.06.002.
White, W.B., 1981. Reflectance spectra and colour in speleothems. NSS Bulletin 43, 20–26.